# Analysis of the Structure of Intramembrane Particles of the Mammalian Urinary Bladder

J. DAVID ROBERTSON and JUAN VERGARA
*Department of Anatomy, Duke University School of Medicine, Durham, North Carolina 27710*

ABSTRACT The luminal and discoid vacuole membranes of the superficial cell layer of the transitional epithelium of the mammalian urinary bladder have been studied by thin-sectioning and freeze-fracture-etch (FFE) electron microscope methods. For the FFE studies membranes were deposited on a cationized glass surface, covered by a thin copper disc, and fractured under liquid $N_2$. Specimens were etched at −100°C and replicated at −190°C. A model of the lattice membrane derived from thin sections was used to predict the heights of the fracture faces above the glass surface. A hexagonal pattern of globular intramembrane particles spaced 160 Å apart was seen in the external fracture (EF) face plaques as previously described and regarded as the dominant structure. However, very extensive areas of another pattern, seen before in only limited areas, have been found in the EF faces. The pattern consists of a smooth hexagonal lattice with the same space constant as the globular one but a different structure. By image analysis it consists of overlapping domains bordered by shared but incomplete metal rims. Each domain has a central spot of metal encircled by a shadow. The surface of the smooth lattice is partly complementary to the corresponding protoplasmic fracture (PF) face which shows a similar hexagonal lattice with the same space constant. The height of the smooth EF lattice above the glass substrate is the same as the plane of the center of the lipid bilayer predicted by the model. The mean heights of the particles of the globular EF lattice are greater than the total thickness of the membrane as predicted by the model and confirmed by measurements. The globular EF lattice is not complementary and it is concluded that the globular particles do not exist in the native membrane but arise artifactually during the preparatory procedures.

Porter and Bonneville (36) first noted the unusual features of the luminal membrane of the mammalian urinary bladder epithelial cell, and it subsequently has been the subject of numerous investigations by groups associated with Porter (11, 12, 33, 37, 47) and Hicks (22–27, 29, 42, 56, 57), by ourselves (30, 38, 53, 54), and others (28). It is now established that 70–75% of the surface area of the luminal membrane and the membranes of the related discoid vacuoles in the luminal epithelial cell display external plaques 0.2–0.5 μm in diameter comprised of particles in hexagonal array with p6 plane group symmetry spaced ~160 Å center-to-center. In negatively stained preparations each particle consists of six subdomains, each divided into two parts, arranged around a central depression or hole ~20 Å in diameter. The interplaque membrane has the ordinary unit membrane appearance in sections and is ~75 Å thick, whereas the plaque membrane is ~120–130 Å thick. The plaques are relatively stiff while the interplaque membranes are more flexible and are often sharply folded, particularly in the discoid vacuoles. For this reason the interplaque membrane is frequently called the "hinge" membrane to distinguish it from the "plaque" or "lattice" membrane.

In freeze-fracture-etch (FFE) preparations the ~120 Å surface particles have a counterpart in an array of globular particles in the external fracture (EF) faces (8, 42). The EF particles usually appear globular and have been said by Staehelin et al. (47) to rise 40 Å above the EF face and to fit into corresponding pits in the complementary protoplasmic fracture (PF) faces. They do not protrude into the protoplasmic surface which appears smooth in FFE preparations (47, 30). The EF and PF faces have thus been considered complementary.

We have studied a purified fraction of the membrane by the FFE technique. Membranes attached to glass were fractured and the heights of fracture faces above the glass surface were calculated from measured shadow lengths. We have used a



THE JOURNAL OF CELL BIOLOGY · VOLUME 86 AUGUST 1980 514-528

model derived from thin sections to predict the heights. We have found two kinds of lattices in the EF faces, the previously observed globular particle lattice and extensive areas of another smooth lattice, resembling one observed in only very limited areas earlier by Staehelin et al. (47). The latter corresponds in height to the center of the bilayer as predicted by the model and is nearly complementary to the PF faces. The mean height of the particles of the globular EF lattice projects 163 Å above the glass, and the globular EF face is not complementary to the PF face. We conclude that the globular particles are preparatory artifacts.

## MATERIALS AND METHODS

### Isolation of Hexagonal Membranes

The terms "hexagonal membrane" or "lattice membrane" are used to refer to the membranes with plaques containing hexagonal lattices of particles. Hexagonal membranes from cow urinary bladder were isolated by the procedure described by Vergara et al. (55) with slight modifications to be described elsewhere. This procedure involves isolation by sequential banding in two-step sucrose gradients whereby the material "zoning" at 32% wt/wt sucrose (density = 1.13 g/m) consists of highly purified hexagonal membranes. The procedure employs only a sucrose solution in Tris-HCl buffer at pH 7.4 and avoids any extractive agent.

### Freeze-fracture

Preparations were made on round glass coverslips 12 mm in diameter by a method adapted from Fisher (14). 0.25 ml of membrane suspension (0.5 mg/ml of membrane protein) was centrifuged onto the glass surface cationized with 0.1% Alcian Blue (46). Excess membranes were washed off with distilled deionized water. The glass was then covered with a flat thin copper disc 8–10 mm in diameter and ~200 μm thick with a protruding handle. The copper "frying pan" was etched with nitric acid. The excess water was blotted and the preparation, held with forceps by the glass rim only, was frozen by mechanical insertion into propane at −190°C using a rapid freezing device constructed by Costello and Corless (13). Fracture was performed at liquid nitrogen ($LN_2$) temperature, either by hand in $LN_2$ at atmospheric pressure or at $\sim 5 \times 10^{-8}$ torr in the $LN_2$ cooled (−190°C) stage of a Denton FFE apparatus (Denton Vacuum Inc., Cherry Hill, N. J.) mounted on an ionization pump. The specimens were either etched (freeze-dried) at −100°C for ~45 min or, if fractured under high vacuum, replicated at −190°C without etching. Replication was performed at −190°C at an initial vacuum usually $\sim 5 \times 10^{-8}$ torr. Pt-C was deposited by arc sublimation from 75 mm at an angle of 20° for 10 s, then carbon vertically for 15 s. The replicated film was floated on 50% hydrofluoric acid, cleaned in Chlorox, and mounted. Control preparations on glass were studied by freeze-drying without fracturing.

Some preparations were prepared in the conventional fashion in a Balzers 360 FFE unit (Balzers Corp., Nashua, N. H.) using resistance electrodes. Thin sheets of freshly microdissected bladder epithelium mounted between thin films of copper (19) were propane frozen (13).

No cryoprotectants or fixatives were used in any of the procedures employed.

### Electron Microscopy

Micrographs were taken at about × 40,000–50,000 using an AEI 801, Siemens Elmiskop 102, or Philips 301 electron microscope. Tropomyosin crystals were used for calibration. Optical diffraction patterns and filtered images were made by Mr. W. Voter in Dr. Harold Erickson's laboratory in the Department of Anatomy. All FFE micrographs are printed in reverse contrast (shadows black).

### Measurements of Height

The heights of the membrane structures were calculated in selected areas in stereoscopic micrographs taken at about × 40,000 at 0°, +20°, and −20°. Membrane areas were selected for measurement that were not artifactually turned up from the substrate. Shadow lengths were measured parallel to the shadowing direction.

The part of the 12-mm coverslip on which we deposited our specimens, from which we took replicas at random for study was ~8–10 mm in diameter. No effort was made to compensate for the ±5 mm variations in the shadowing angle because of the exact location of the specimen used. This could make a difference of ±0.8° in the shadowing angle, introducing an error of about ±5% in the measurements. The shadow lengths are influenced by the thickness of the replica, in that the measured length is approximately the result of the mean of the zero and final value of the metal thickness. This could increase the measured heights ~5% if the vertical metal thickness is 10 Å.

Another potential source of error is departure from flatness of the coverslip surface. However, we have detected no such deviations and the internal consistency of our data suggests that the surfaces are flat.

So far we have not studied complementary fracture faces. We have examined ~600 specimens.

## RESULTS

### Thin Sectioning

In sections, the hinge membrane has the usual unit membrane appearance and is ~75 Å thick. The lattice membrane is similar but has a layer of densely staining particulate material added to the outer dense stratum. In edge-on views, individual particles may be clearly seen, as in Fig. 1 *a*. Each particle is ~65 Å high by ~100 Å wide, and they are spaced at a period of ~140 Å. The overall membrane thickness including the particles is 130 Å (Fig. 1 *b* and Table I). The hinge membrane thickness of ~75 Å was measured in other micrographs. We expect shrinkage in sections and we wish to compare measurements made in sections with ones made in freeze-dried material. Severs and Warren (42) measured the diameter of the external particle in freeze-dried material to be 121 ± 21 Å. We measure this value to be ~100 Å in Fig. 1, suggesting shrinkage of 13%. We have measured the mean thickness of the hinge membrane freeze-dried on glass to be 86 Å. In sections, the corresponding figure is 75 Å, 15% less. Thus we estimate shrinkage to be 15% and correct the values in Table I accordingly. Individual components, of course, may not shrink this much or not at all.

Thin sections of the purified fraction show irregularly folded sheets of membranes of varying size that may fold into vesicles with the particle arrays directed either outward or inward.

### Freeze-fracture-Etch

#### External Surface

Fig. 2 shows an unfractured membrane adhering to the glass by its protoplasmic surface (PS). The external surface (ES) particle lattice is revealed by freeze-drying. Several plaques (*P*) are seen. A few scattered individual particles lie free. These cast sharp shadows (left three small arrows). The membrane between the plaques is the hinge membrane (*) seen in sections as ordinary ~75-Å unit membranes free of particles. It is unusual to see particles detached from the plaques lying free in the hinge membrane surface as in this picture. They show a central depression and cast shadows of the same lengths as the ones at the edges of the plaques. In flat areas we measure the individual particle heights above the hinge membrane surface as 53 ± 10 Å (50 particles). This is less than the ~75-Å figure predicted for the particle thickness in Table I but here we are measuring to the ES of the hinge membrane instead of to the bilayer core. From the shadows cast by the particle-free hinge membrane onto the flat glass surface as at the small arrow on the glass surface to the right, the thickness of the hinge membrane (*) in this micrograph is 83 Å.

The central part of the area labeled *P* in Fig. 2 is enlarged in Fig. 3 *a*. Its diffraction pattern is shown directly in Fig. 3 *b* and through the filtering mask in Fig. 3 *c*. The filtered ES image is seen in Fig. 3 *d*. The particles show up as rings of metal surrounding a central depression. Six subunits, each ~30–40 Å in diameter, are seen in each particle although the ones toward the shadowing source are less clearly resolved. Dark shadows delineate the particles. Two adjacent particles are

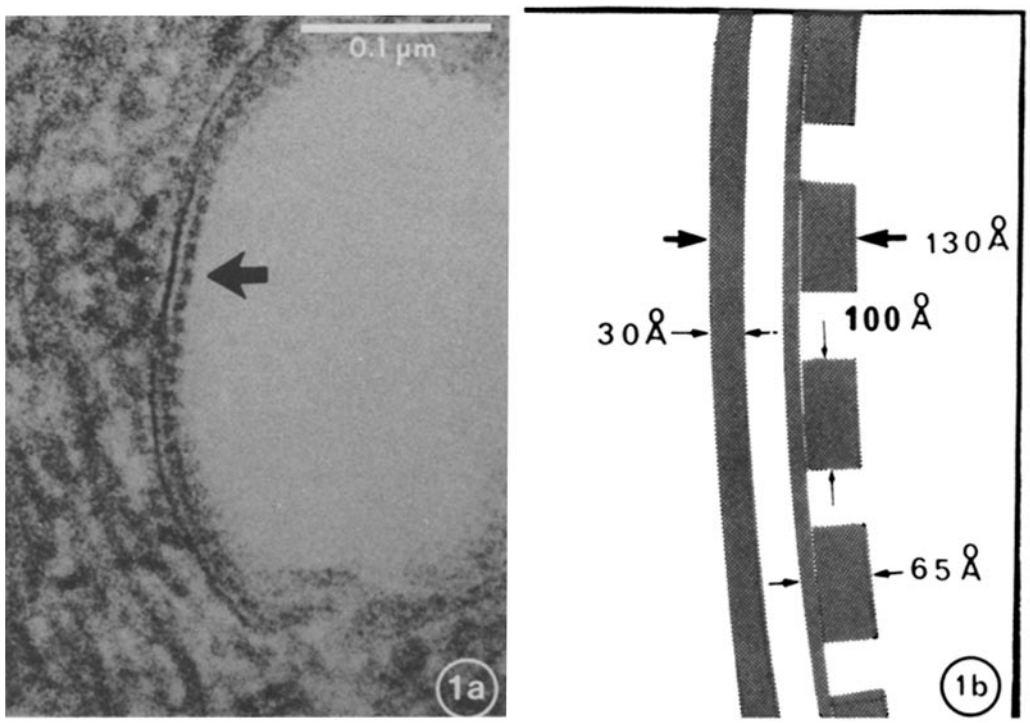


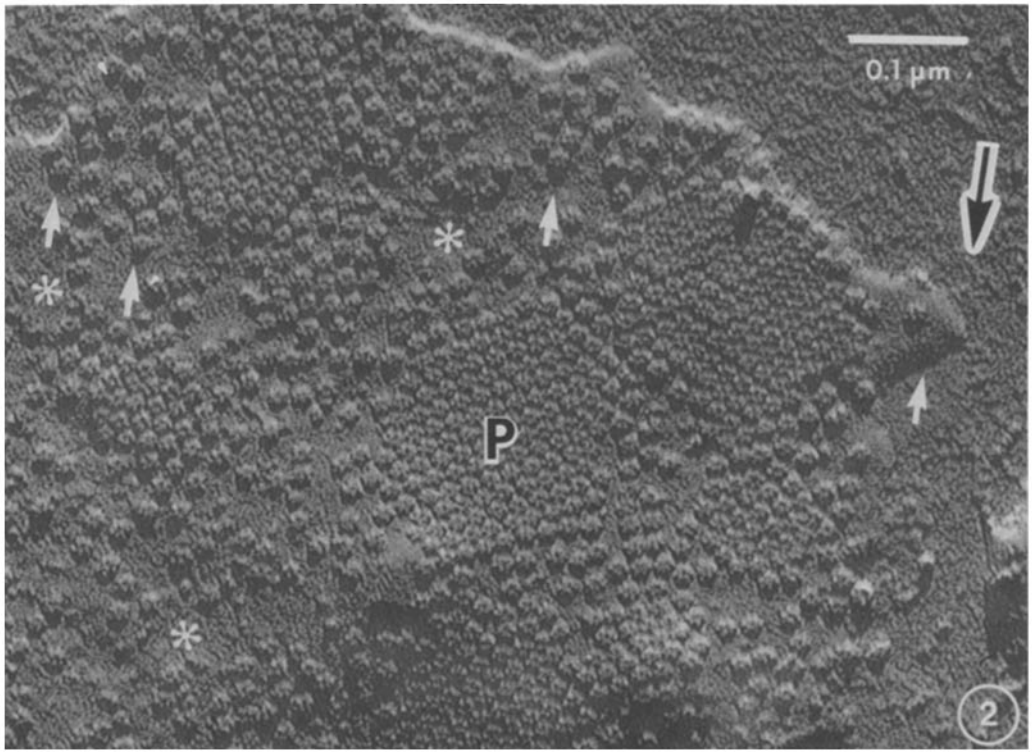


FIGURE 1 (a) Transection of membrane of a fusiform vacuole showing the particle lattice in profile. The region designated by the arrow is enlarged diagrammatically to the right in *b*. The preparation was fixed in glutaraldehyde-$OsO_4$, acetone dehydrated, Epon embedded, and sectioned with a diamond knife. Uranyl and lead stained. × 248,000.

FIGURE 2 A replicated unfractured freeze-dried lattice membrane attached to glass with the ES particle lattice (*P*) up. The shadowing direction is indicated with an arrow to the upper right in this and other FFE micrographs. × 160,000.

encircled in *a* and *d* and their centers, separated by 160 Å, are indicated.

## EF Faces

LATTICE MEMBRANE: Figs. 8–12 illustrate the EF faces observed in the isolated bladder membranes fractured on glass and deeply etched. The EF plaques display two distinctly different types of patterns. One is a globular pattern (*GP*) characterized by arrays of globular particles rising from the membrane matrix. This kind of pattern is the one most commonly seen and is like the ones previously described (30, 42, 47). The other is a smooth pattern (*SP*) made up of a delicate

TABLE I

*Membrane Parameters in Sections*

| | Measured in sections | Corrected for shrinkage |
|---|---|---|
| | Å | |
| Membrane thickness | 130 | 150 |
| Particle thickness | 65 | 75 |
| Hydrophobic core | 35 | 40 |
| Protoplasmid dense stratum | 30 | 35 |
| Overall hinge membrane thickness | 75 | 86 |

lacey array of rows of metal in which individual particles are not apparent. The rows in Fig. 8 are ~120 Å wide and repeat at a period of ~140 Å. The smooth lattice sometimes dominates the picture as in Fig. 12 but the globular lattice more often dominates as in Fig. 11. Both kinds of lattice sometimes occur in the same plaque. In such cases no sharp boundaries delimit either type of pattern and no change in the direction of the main rows occurs. This is illustrated by the plaque with the aligned arrows in Fig. 8 and the plaque labeled *SP* in Fig. 10. Sometimes the two types of lattice are seen in adjacent plaques as in Fig. 9. In both kinds of structure, either particles or domains are present in hexagonal close packing with a center-to-center spacing of 160 Å.

Optical diffraction patterns (*insets*, Fig. 9) show that both kinds of structures share the same unit cell dimensions. Each shows, however, a characteristic distribution of intensities of the diffracted spots. The coarse globular particle lattice to the right in Fig. 9 gives six equally strong first-order spots (1, 0) of a hexagonal lattice with higher-order spots of diminishing intensity. The absence of asymmetry caused by unidirectionality of the shadowing indicates that decoration plays a significant role in the pattern, even though the shadowing mechanism appears dominant. The diffraction pattern from the smooth lattice to the left shows weaker first-order spots (1, 0) relative to the globular pattern with two spots absent perpendicular to the shadowing direction. This indicates that the shadowing mechanism is dominant in the formation of the image. The 2, 0 spots of the smooth lattice are of about the same intensity as the 1, 0 spots but the 1, 1 spots are of distinctly higher intensity. The equivalent positions of the 1, 0 spots from both kinds of patterns indicate that the unit cell is the same. However, the altered intensities of the higher-order spots in the case of the smooth lattice indicate the presence of structural features in the smooth pattern that are absent in the globular one. The very strong 1, 1 spots suggest a higher concentration of mass in the center of each domain in the smooth lattice. The nature of this is best understood by image analysis. Superficial examinations of the micrographs by sighting along the lattice obliquely in micrographs like Fig. 8 give the impression that the repeating unit is a double row of raised ridges with a depression between them. Image analysis confirms this and shows that it is rows of individual roughly annular domains each of which has a depressed center with an elevated central metal spot. The individual domains (arrows) can be made out directly in Fig. 4*a*. The diffraction pattern from this area is shown directly in Fig. 4*b* and through the mask used for filtration in Fig. 4*c*. The filtered image is shown in Fig. 4*d*. Here a hexagonal array of clearly defined domains (arrows) is apparent. Each shows up as an incomplete annulus of metal surrounding dark shadows. One of these is cast by the elevated annular edge of the domain in the line of shadowing and the other by a raised structure coated with metal in the center of the domain. Only the edges of the domains perpendicular to the shadowing direction show up and the edges are shared by adjacent domains. The center-to-center spacing of the domains is ~160 Å (arrows). The shared metal annular ridges delineating the domains are 20–25 Å wide and the central spot of metal is ~20–25 Å in diameter.

Another difference between the globular and smooth lattices is best seen in stereo micrographs (not shown) in which the globular particles can be seen to lie in a plane distinctly higher than that of the smooth lattice.

We have also studied membranes fractured on glass at −190°C and replicated immediately without etching (not illustrated). In these the fractured membranes are surrounded by amorphous ice of variable thickness which prevents measurements directly to the glass surface. The EF faces also show the globular lattice in association with the smooth lattice and in places transitions from one type to the other. Both lattices occur with about the same frequency as in the specimens described above.

In whole cells, the dominant picture in the EF face is that of the globular lattice. However, the smooth lattice does occasionally occur in limited areas as noted previously (47). In Fig. 13 we see an area (arrows) in the convex EF face of a discoid vesicle in which the smooth lattice is clearly identifiable. This micrograph is of an unetched whole cell preparation frozen in propane by the method of Gulik-Krzywicki and Costello (19) in the Balzers 360 apparatus. Thus the smooth lattice is not simply a product of the glass-fracturing technique, the prolonged etching, or some peculiarity of the apparatus used. It is demonstrable in intact cells but seems to be unstable and easily converted to the particle lattice.

The relatively featureless areas between adjacent plaques marked with asterisks in Figs. 8 and 10–12 are the hinge membrane EF faces. These areas are relatively extensive in Figs. 8, 10, and 11, making up ~25–30% of the total membrane area (42). In Figs. 9 and 12 they are distinctly reduced. In Fig. 9 they are so narrow as to be hardly distinguishable. Indeed, the two plaques marked *SP* and *GP* can only be seen as separate ones by sighting diagonally along the rows and noting that there is a sharp break in direction in the line of transition from the smooth to the globular lattice. Such marked reduction in the area of the hinge membrane has only been seen in the isolated membranes.

## PF FACES

LATTICE MEMBRANE: In the material fractured on glass and etched we have frequently seen sheets of membrane with no identifying features. These were about the same size and were found with about the same frequency as the clearly identifiable lattice membranes. It became apparent after studying the specimens on glass replicated without etching that these amorphous membranes were the protoplasmic membrane halves because they had the features seen in Figs. 5 and 6. The PF faces are known to be very sensitive and to rapidly lose their identifying features during etching (42, 47). These micrographs showed the typical appearance of the plaques in the PF faces. They were the same size, shape, and distribution as the plaques in the EF faces but uniformly had the appearance in Figs. 5 and 6 when shadowed at a low angle. This is the pattern previously described (30, 42, 47) as one of "pits" complementary to the EF globular pattern. We have analyzed this pattern by optical diffraction and found that it is more complicated. By viewing

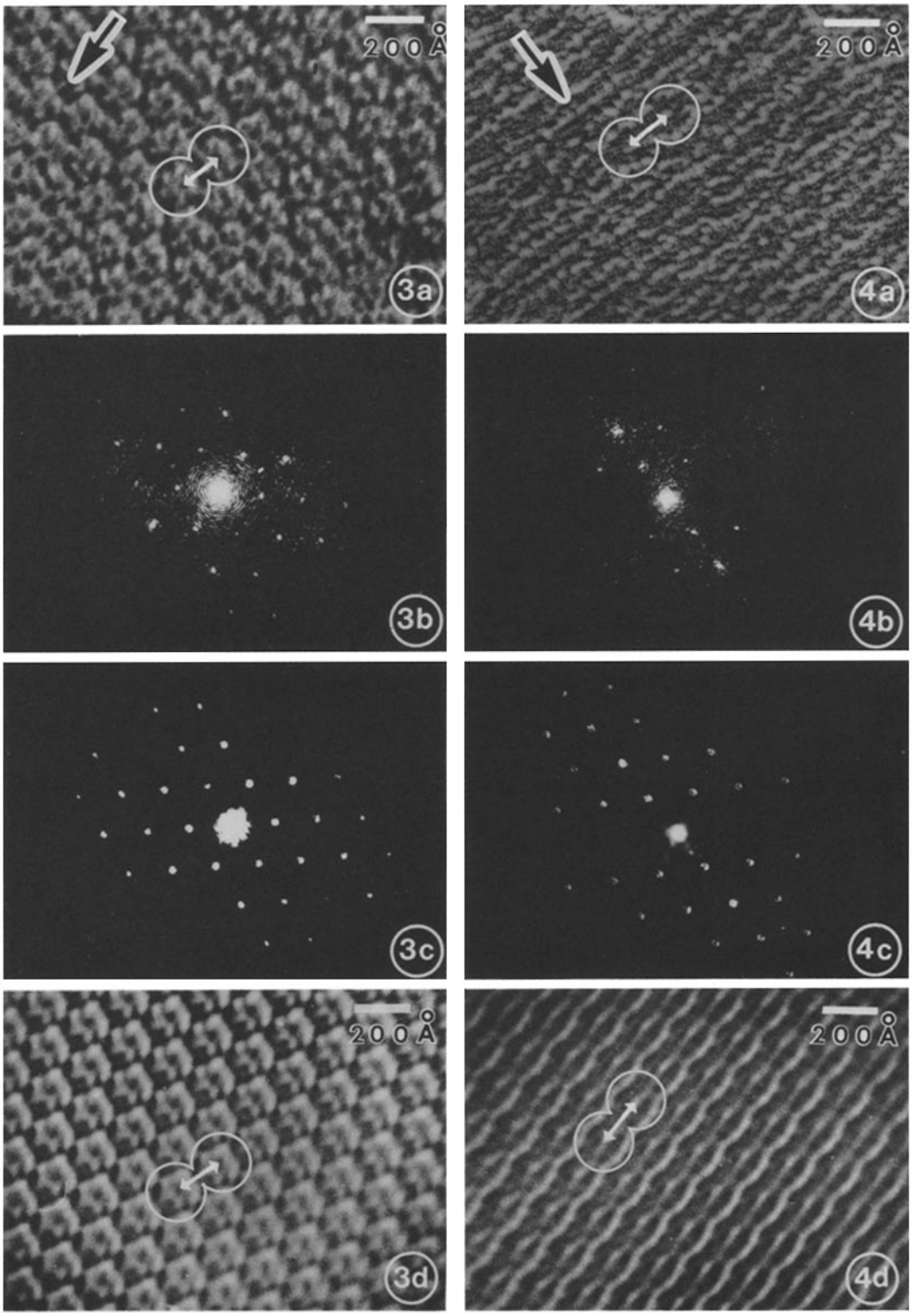


FIGURE 3 (*a*) Enlargement of the area designated by *P* in Fig. 2. × 430,000. (*b*) Optical diffraction pattern obtained from a circular area including most of the plaque labeled *P* in Fig. 2. It is slightly underexposed to show the central spots. (*c*) The diffraction pattern through the mask used for filtration using a longer exposure to show up the peripheral spots. (*d*) The optically filtered image. Note the central depressions in each particle spaced at a distance of 160 Å. Each particle is hexagonal and contains six subunits. The particles are each surrounded by shadows. Two particles are encircled and their centers designated by the arrows as in *a*. × 430,000.

FIGURE 4 (*a*) High magnification micrograph of a portion of the EF face of a plaque like the one designated *SP* in Fig. 9. (*b*) Underexposed diffraction pattern from *a*. (*c*) Diffraction pattern through the mask used for filtration. The exposure was longer than in *b* so that all the spots used show up. (*d*) Filtered image. Compare with Figs. 3 *d* and 7 *d*. Mag. (*a* and *c*) × 440,000.

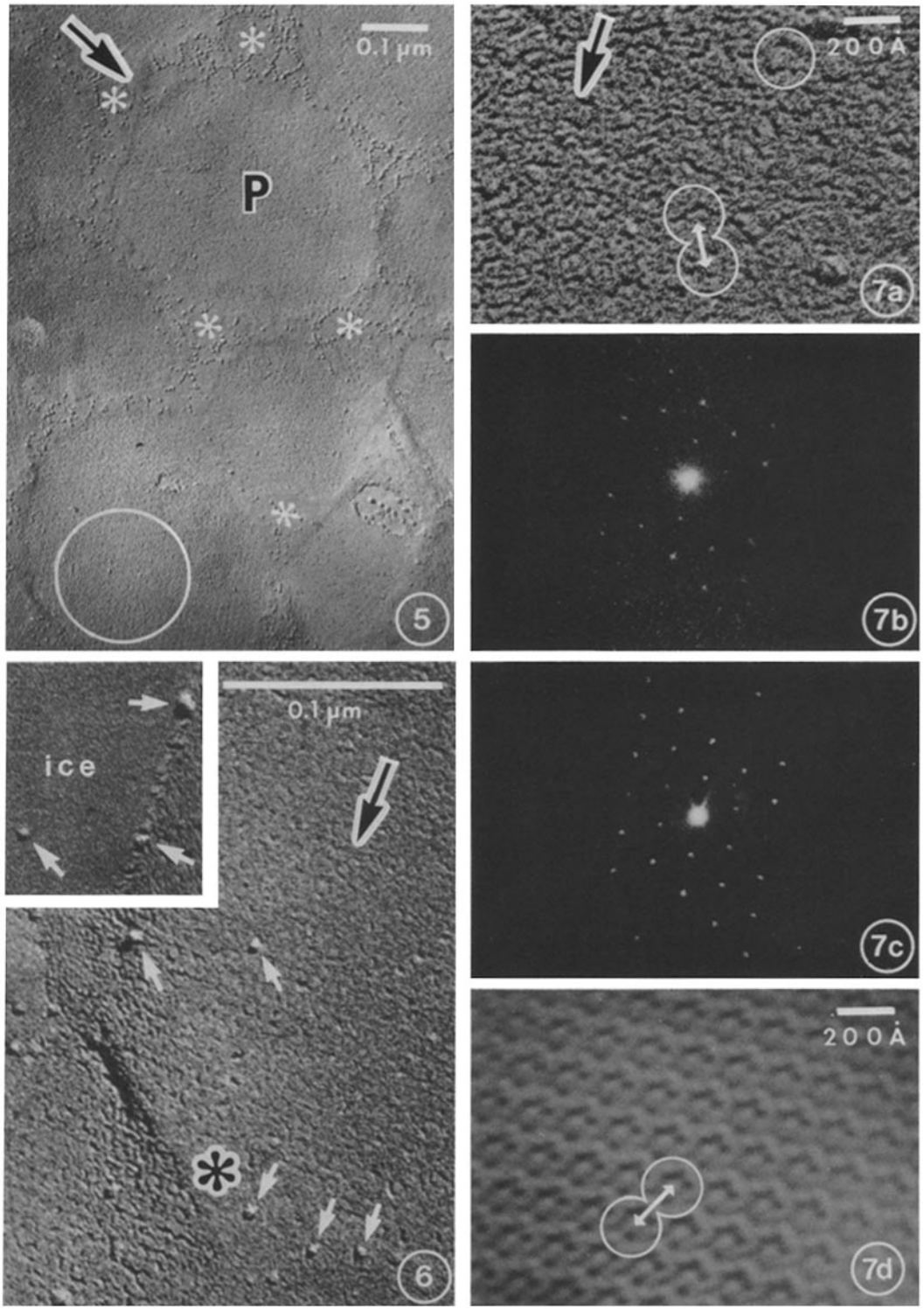


FIGURE 5 Area of the PF face in a preparation made from the intact bladder epithelium. It was fractured in the Balzers 360 and not etched. Several plaques (*P*) are seen separated by areas of intervening hinge membrane designated by the asterisks. Moderate numbers of particles ranging in diameter from 50 to 80 Å are seen concentrated primarily on the hinge membrane surfaces, though some are seen on the PF surfaces. The encircled area was used for image reconstruction in Fig. 7. × 100,000.

FIGURE 6 Area similar to the one in Fig. 5 from the same specimen. It is printed at higher magnification to show up the kind of particles (arrows) seen on the hinge membrane EF faces and the PF faces in Fig. 5. The *inset* to the upper left is a portion of the same micrograph printed at the same magnification. It shows an area of ice in the bladder lumen intersecting a PF plaque at a sharp angle. Note the particles on the line of junction of ice and the PF face (arrows to right) as well as the one on the ice (left arrow). × 330,000.

FIGURE 7 (*a*) Enlargement of part of the plaque area encircled to the lower left in Fig. 5. Two adjacent and one individual domain are encircled and the centers of the adjacent ones are indicated by arrows. Each domain consists of an annulus of metal separated perpendicular to the shadowing direction by shadow from a central metal area. The underexposed diffraction pattern in *b* was obtained from the circled area in Fig. 5. (*c*) Diffraction pattern in *b* seen through the mask used for filtration exposed longer to bring out all the spots. The image in *d* was constructed by filtration. (*a* and *b*) × 440,000.

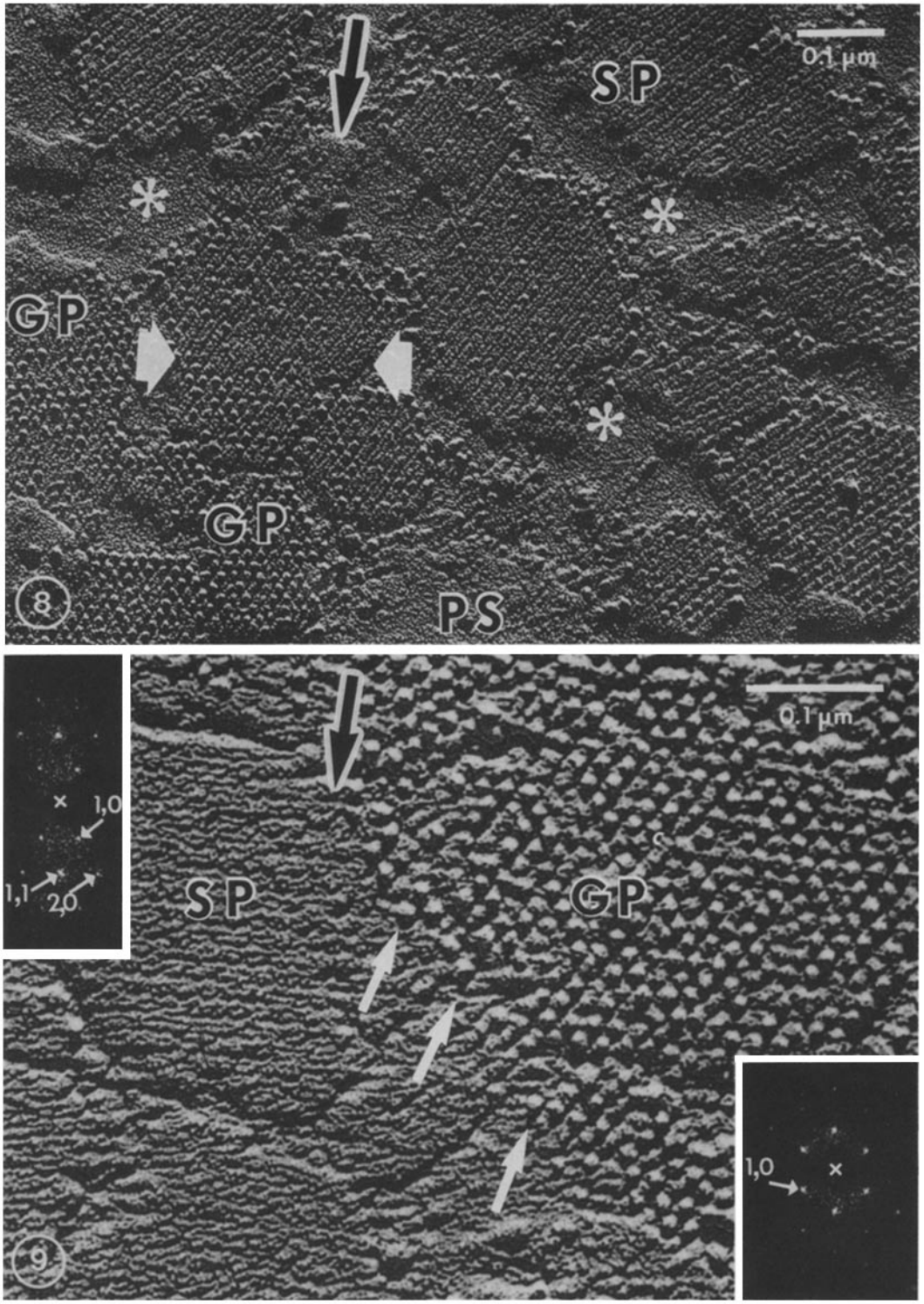


FIGURE 8 Lattice membrane fractured on glass displaying EF face. In the lower center a plaque is seen which did not fracture and thus displays a PS. × 128,000.

FIGURE 9 EF face of the lattice membrane on glass. The smooth pattern (*SP*) is seen to the left and the globular pattern (*GP*) to the right in closely adjacent but separate plaques. × 212,000.

Figs. 5–7 *a* from a small angle one can easily see a regular pattern, but its exact nature is difficult to define in direct images. This is, however, easily done in filtered images.

The area in Fig. 5 encircled to the bottom left is enlarged in Fig. 7 *a*. Note the characteristic domains (circles) separated by 160 Å (arrows). Each consists of a ring of metal surrounding an incomplete dark shadow which surrounds a central metal spot. This is best seen in the filtered image (Fig. 7 *d*). The image is distorted by the unidirectionality of the shadowing, but it is clear that the unit cell is the same as the one in Fig. 4 *d* from a smooth EF face with which it should be compared. As in the EF face, the repeating domain in the PF face also

consists of an annulus of metal surrounding a ring of shadow around a central spot of metal. The annulus is incomplete in the EF face and complete in the PF face, but otherwise the patterns are similar. Each of the surfaces contains regular arrays of material that constitute repeating domains. In both cases the domain contains a central raised spot of metal surrounded by a shadow, indicating a depressed ring. The depressed rings of the two surface domains are mirror images of one another. The rest of the domains are roughly complementary. They differ only in the incompleteness of the outer ring in the EF face and the widths of the outer rings and central spots. In the PF face the outer annulus is thicker (~40 Å) and the central spot larger (~60 Å) than the corresponding structures in the EF face. Fig. 16*b* shows diagrammatically the features of the EF and PF domains in profile view. The aligned arrows point to the raised central spots of the EF domain below and the PF domain above.

HINGE MEMBRANE: The hinge membrane areas in Figs. 5 and 6 (*) are of about the same proportional area as found by Severs and Warren (42) in glutaraldehyde-fixed intact cells.

The PF faces of the hinge membrane in nonetched material sometimes appear smooth and featureless, but sometimes they are covered by numerous small particles 50–80 Å in diameter either randomly distributed or in irregular rows as in Fig. 5. This type of particle also appears on the plaque PF faces (Figs. 5 and 6). The particles indicated by the three lower arrows in Fig. 6 lie on the hinge membrane PF face (*). The ones designated by the two arrows to the upper left center are on the lattice PF face. The *inset* to the upper left is another area in the same micrograph in which a fractured ice surface was identified and interpreted as lying in the bladder lumen. Note the particles designated by the arrows. The one to the left is like the ones seen on the hinge membrane and plaque membrane PF faces. The other two are localized to the boundary between the ice and the membrane fracture face. The upper one seems to be two particles lying close together. There were a moderate number of such particles on the ice surface, but they were not closely spaced.

UNUSUAL PLANES OF FRACTURE: It is generally accepted that fracture planes do not normally run along membrane surfaces (4, 6, 7, 9, 34, 35) even though they may sometimes do so as shown by Hereford and Northcote (21). However, as indicated diagrammatically in Fig. 14, unusual fracture planes frequently occur in our material. Fig. 10 is a replica of the fractured remains of a flattened vesicle with the particulate lattice everted and stuck to the glass. Before fracture, a cross section of this vesicle and the glass roughly in the plane indicated by the diagonal dashed line would look diagrammatically somewhat like Fig. 14. After fracture, the remaining replicated structures are shown diagrammatically in cross section in Fig. 15.

Most of the fractured surfaces in Fig. 10 represent the EF faces of the lattice membrane. These show mostly the rough globular pattern (*GP*), but in some places the smooth pattern (*SP*) is seen. The surfaces labeled *PS* lie above the EF faces and in correct orientation cast shadows onto them. We identify some of them as the smooth unfractured PS of the underlying fractured membranes. The rather large sheet of membrane-labeled PF to the lower left center lies above the surface below it labeled *PS* and is the PF face of the membrane of the top side of the collapsed vesicle. Although in the diagram we show this as a lattice membrane some parts of it are probably hinge membrane. The small membrane fragments upon it (arrows *1*) cast shadows of the right length and are about the right size and shape to be hinge membrane halves as may be appreciated by comparing them with the hinge membrane EF faces (*) elsewhere. The unlabeled arrow on the PF face points to a structure that could represent a part of the same membrane half as the fragments indicated by arrows *1*, but which we cannot identify with certainty. There is no evidence of the characteristic PF face pattern of the lattice membrane. To the upper center in the area marked *PS* one sees a special feature at arrows *2* and *3*. The part of this surface bordering the globular EF lattice to the lower left is the protoplasmic surface of the lattice membrane just below, which was only partially fractured. Note the bands of lighter and heavier accumulations of metal in the regions indicated respectively by arrows *2* and *3*. The metal is thinner at arrow *2* and thicker at arrow *3*. The changes indicate a change in membrane thickness. They are caused by the transition from a thicker lattice membrane (*PS*) above arrow *2* to a narrow band of intervening thinner hinge membrane and back to the thicker lattice membrane below arrow *3* in an adjacent placque.

The particles of varying size scattered irregularly on the unfractured membrane surfaces and on the glass surface are interpreted primarily as condensation artifacts.

In the material fractured on glass we can refer to the flat glass surface and compute heights by measuring shadow lengths. At arrow *4* to the lower left and arrow *5* to the upper right in Fig. 10 the PS of the lattice membrane casts shadows respectively onto the glass surface and the smooth EF face. Arrow *6* to the lower right indicates the shadow of the unfractured hinge membrane on the glass. Arrow *7* to the left of arrow *6* points to the shadow cast by the rough globular EF face onto the glass and at arrow *8* to the upper left onto a surface that we interpret to be the hinge membrane EF face (*). Fig. 11 again shows the shadow cast by the globular lattice onto the glass surface (broad white arrow and *inset*). Fig. 12 provides an example of the kind of shadow cast upon the glass surface by the smooth lattice (broad white arrow). Note that the rough lattice casts a sharply serrated shadow, while the smooth lattice casts a smooth shadow. The serrated spikes are the shadows of the globular particles. These project above a level defined by the dip between each spike of the serrations. The level from which the spikes rise in Fig. 11 roughly matches the level of the height of the smooth lattice in Fig. 12. Hence the particles rise above the level of the smooth lattice by a distance defined by the spike heights. In some places as at the arrows in Fig. 9 one can see places where the globular particles of the rough lattice cast sharp shadows onto the smooth lattice.

## Classification of Shadowed Structures by Height

As indicated in Fig. 15, several heights above the smooth glass surface or other surfaces, including those mentioned, can be defined. These are each designated by the letter $h$ with a subscript. Nine such heights ($h_1$-$h_9$) are defined in the figure. Three of these ($h_1$-$h_3$) refer to the hinge membrane. $h_1$ is the height of its EF face above the glass. $h_2$ and $h_3$ are the heights of its PS above the glass and its own fracture face, respectively. Because it is thicker and overlaps the hinge membrane, six heights are measured for the lattice membrane. Two of these, $h_4$ and $h_5$, relate its EF surface to the glass (broad white arrow in Fig. 12 and to the fracture face of the hinge membrane, respectively (arrow 8 in Fig. 10). The remaining four heights, $h_6$-$h_9$ relate its PS to other surfaces. The first two, $h_6$ and $h_7$,

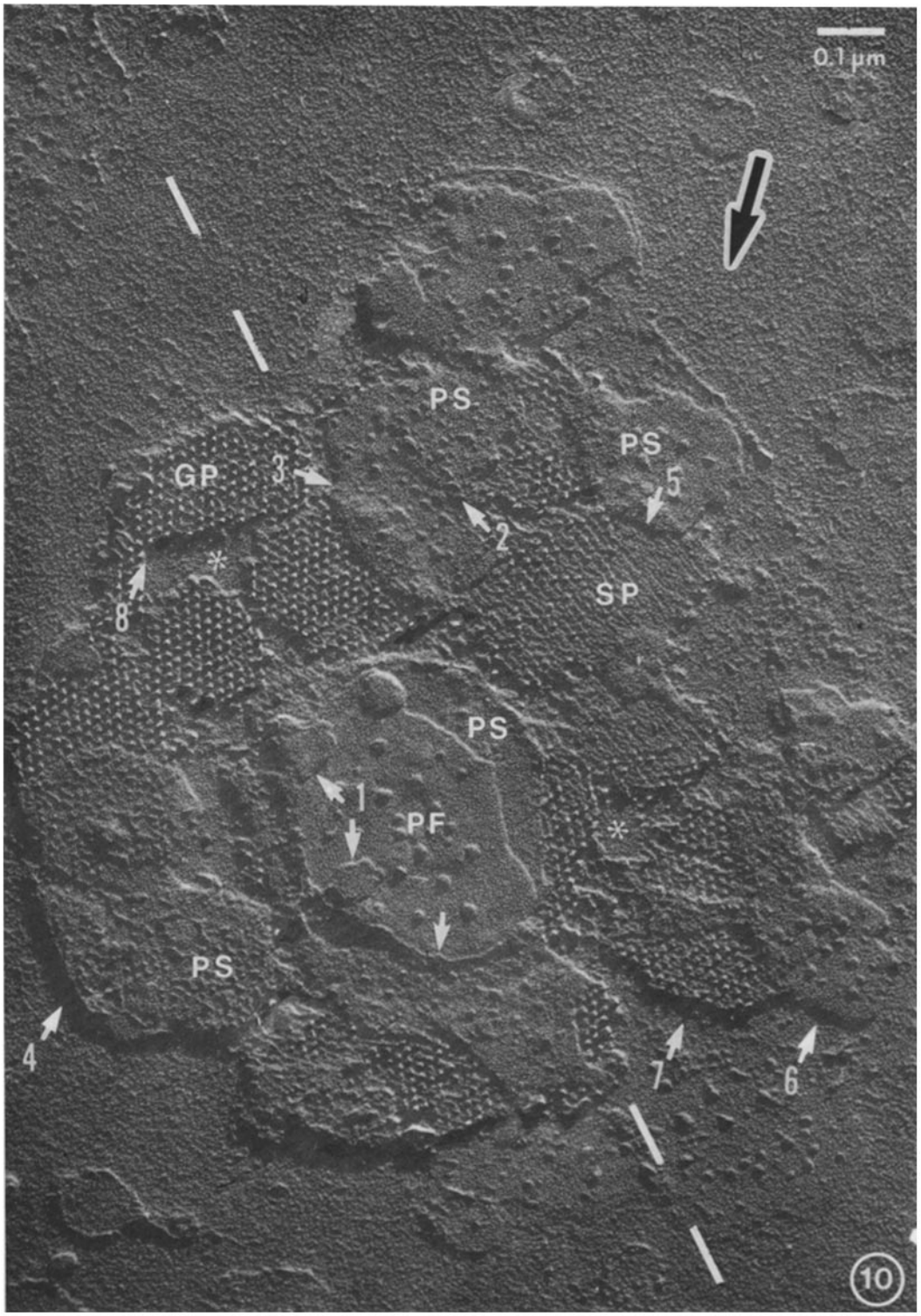


FIGURE 10 Complex fracture of a vesicle. See text. × 103,000.

give its height above the glass and its own corresponding EF face, respectively (arrows *4* and *5* in Fig. 10). The last two, $h_8$ and $h_9$, relate its height, respectively, to the unfractured protoplasmic and EF faces of the hinge membrane.

Fig. 14 is based on a model derived from Fig. 1 *a* as shown diagrammatically in Fig. 1 *b*. The dimensions in Table I are mostly from measurements in Fig. 1 *a*. The hinge membrane, from measurements in other micrographs, is taken to be a simple unit membrane ~75 Å thick. The lattice membrane in Fig. 1 is taken to be a modified unit membrane with the cytoplasmic dense stratum ~30 Å thick and the ~65 Å thick particle lattice making up most of the outer dense stratum, raising the overall thickness to ~130 Å. The figures of 130 and 65 Å represent the maximum thickness in Fig. 1 *a* and they are used in Table I. If the value of 120 Å in the literature for the membrane thickness and a lower value for the particle thickness are used, this makes no statistical difference in our analysis.

We shall now use the dimensions in Table I to predict the

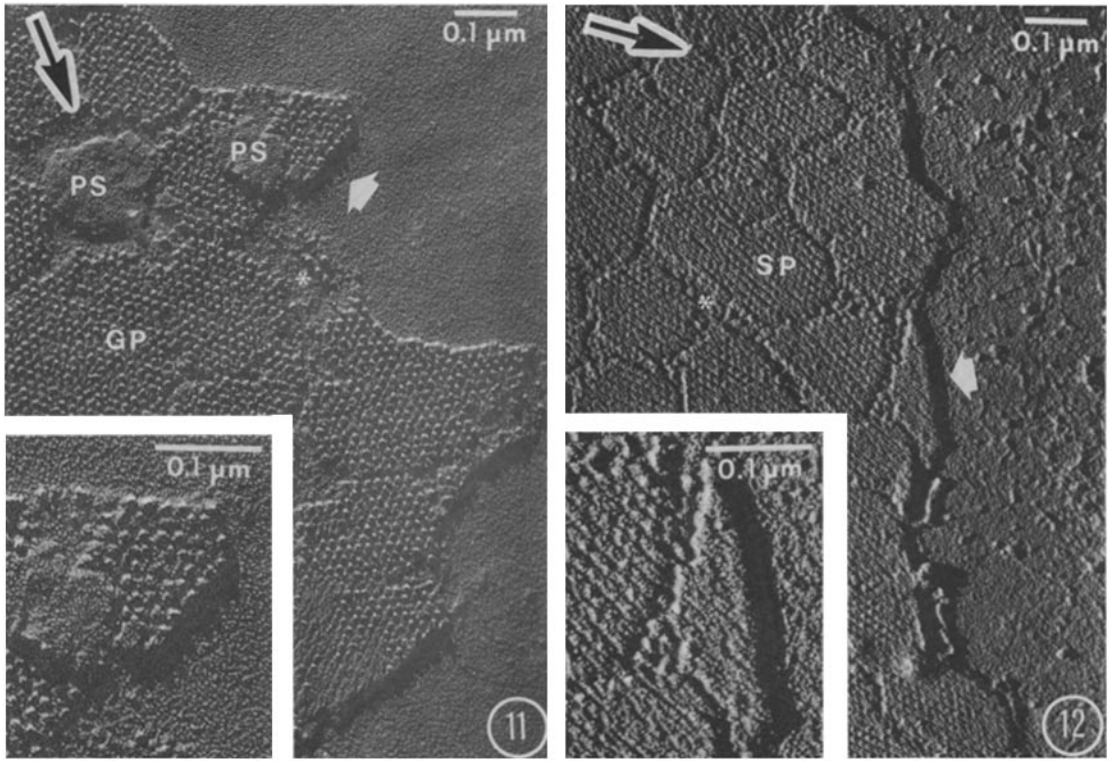


FIGURE 11 EF face of lattice membrane fractured on glass showing mostly the globular pattern (*GP*). The area designated by the broad white arrow is enlarged in the *inset* to show the serrated shadow of the globular pattern on the glass. Two small areas designated PS are patches of membrane that did not fracture and are thus protoplasmic surfaces. × 90,000. *Inset:* × 145,000.

FIGURE 12 EF face of lattice membrane fractured on glass showing the smooth shadow cast by the smooth lattice on the glass (broad white arrow). × 80,000. Inset enlargement is of area near white arrow. × 145,000.

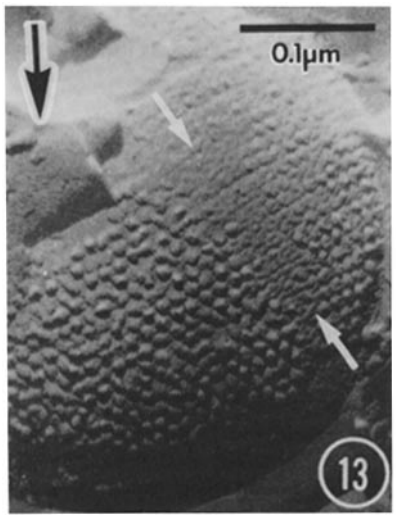


FIGURE 13 Vesicle in a whole cell preparation like the one used in Figs. 5–7 showing the EF face. × 180,000.

heights in Fig. 15. $h_1$ should be half the thickness of the hinge membrane or 43 Å; $h_2$ should be the total thickness of the hinge membrane, i.e., 86 Å, and $h_3$ again half this value; $h_4$ should be the total thickness of the lattice membrane of 150 Å minus 43 Å or 107 Å; $h_5$, the height of the lattice membrane EF face above the hinge membrane EF face should be 107 less 43 or 64 Å. $h_6$, the overall thickness of the lattice membrane, defining the PS, should be 150 Å; $h_7$, the height of its PS above its EF face should be 43 Å; $h_8$, the height of its unfractured PS above that of the unfractured hinge membrane should be the difference between their overall thickness, i.e., 150 less 86 or 64 Å; $h_9$, the height of the lattice membrane PS above the hinge EF face should be 150 less 43 or 107 Å. We have obtained measurements of each of these nine quantities and they are given in Table II along with the corresponding expected values derived from Table I. None of the *P* values are significant. These were derived from the formula of the Student's *t* test and statistical tables (43, 1).

The data in Table II refer only to the idealized model and the smooth EF lattice. What about the globular lattice? We have made three types of measurements on it. First, we measured the maximal heights of the particles above the glass using the peaks of the serrated shadows like those at the broad white arrow in Fig. 11 as the particle heights. The mean of these values is the maximal height of the EF face of the globular lattice and we designate it in Table III as $h_{4a}$. We also measured separately the heights of the troughs betwee the serrated spikes above the glass. The mean of these values is the minimal height of the globular lattice above the glass and we designate it $h_{4b}$. We have of course, corresponding measurements of the same structures in the $h_5$ category, in this case measuring to the fractured hinge membrane surface instead of the glass surface. These are designated $h_{5a}$ and $h_{5b}$. We have made a third type of measurement on the globular lattice. In some micrographs, as in Fig. 9 at the arrows, individual globular particles cast shadows onto the smooth lattice. We thus include them also in the table measurements of such particle heights above the smooth lattice, designating them $h_{5c}$.

The expected values listed in Table III require comment. There is nothing in the model to allow us to make any prediction about the value of $h_{4a}$. However, we can make some

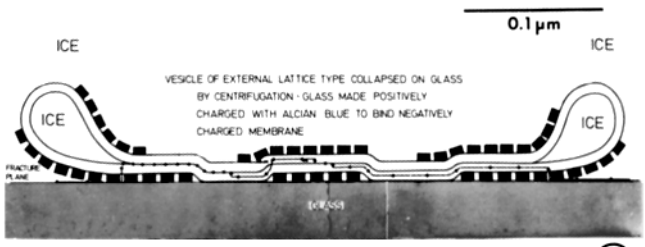


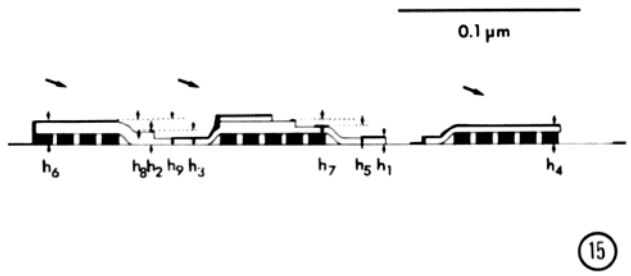


FIGURE 14 Diagram of a lattice membrane vesicle on glass in cross section. The diagram was constructed to indicate the structures that might have been present in Fig. 10 before fracture. Considerable license was taken in constructing the diagram which is a composite. See text.

FIGURE 15 Cross section of the vesicle in Fig. 15 as it would appear after fracture. The fractured remnants lie on the glass surface below. The diagonal arrows indicate the shadowing direction. The scale is the same as Fig. 14 and the diagram does not follow Fig. 14 exactly. To illustrate all the heights (h), license is again taken. See text for further description.

reasonable guesses about the other quantities. Thus, we might guess that the values of $h_{4b}$ and $h_{5b}$ relate to the smooth lattice heights for $h_4$ and $h_5$ in Table II. Hence we assign the expected values of 107 and 64 Å, respectively, to $h_{4b}$ and $h_{5b}$. Having the value of 163 Å for $h_{4a}$, we might expect the value of $h_{5a}$ to be this figure less the 43-Å thickness of the fractured hinge membrane. Hence we assign to $h_{5a}$ an expected value of 120 Å (163 less 43 Å). Finally, if the globular particle is a structure added to the smooth lattice, we might expect its height above the smooth lattice to be the difference between the mean height of the rough particle lattice (163 Å) and the predicted height of the smooth lattice (107 Å). Thus we predict the $h_{5c}$ value to be 56 Å.

Note that the mean maximal height of the particles above the glass in the globular lattice areas, $h_{4a}$, is 163 Å, more than the total thickness of the intact lattice membrane. Also note that the heights of the globular particles vary greatly, reaching as high as 234 Å, much more than the total lattice membrane thickness. The corresponding $h_5$ values are easier to compare with the $h_4$ values if corrected to the glass surface by adding the 43-Å thickness of the fractured hinge membrane as indicated in Table III. Note that the height of $h_{5a}$ corrected to the glass is 161 Å, very close to the 163 Å value of $h_{4a}$. These are the means of two separate sets of over 200 measurements each and this is the kind of agreement one might expect if we are correctly identifying the surfaces on which the shadows are projected. This agreement thus confirms our identification of the hinge membrane EF faces. If the areas identified as hinge membrane EF faces were sometimes glass surfaces, such close agreement would not be expected. It is also revealing to compare the value of $h_{5b}$ corrected to the glass, 119 Å, to the separately measured value of 120 Å for $h_{4b}$. These values are also remarkably close, even though the numbers of the two sets of measurements are smaller. Again the agreement supports our identification of the hinge membrane EF faces. Note that the minimum heights of the globular lattices in both these sets of measurements, 120 and 76 Å, are both reasonably close to the mean values of 108 and 69 Å for the smooth lattice in the $h_4$ and $h_5$ categories in Table II. This suggests that the troughs between the spikes in the rough lattice correspond to the surface of the smooth lattice. The particles measured at the boundaries between the smooth and globular lattices seem to be the same structures as the spikes in the serrated edge shadows (Fig. 11). Adding the average particle height figure of 55 Å to the globular lattice minimum height should, if this interpretation is correct, give the value of the maximum globular lattice height. In the $h_{4b}$ case adding 55 to 120 gives 175 Å, close to the 163 Å value in $h_{4a}$. Similarly, in the $h_{5b}$ case, adding 55 Å to the measured value of 76 Å gives 131 Å, again not far from the measured $h_{5a}$ value of 118 Å.

From the above it becomes quite clear that the spikes of the globular lattice must be something built up upon, expelled from, or pulled out of the smooth lattice during fracturing or replication. The height of the troughs between the spikes is slightly higher than the height of the undisturbed lattice surface just as might be expected if the particle is derived this way. In any case it is clear that the particles and spikes are the same thing. They obviously represent something added to or derived in some way from the smooth lattice during fracturing or

TABLE II

*Parameters of Hinge and Smooth Lattice Membranes in Metallic Replicas on Glass*

| Designation | No. of measurements | Mean | Range | Expected value | *P* |
|---|---|---|---|---|---|
| | | | Å | | |
| Hinge membrane heights | | | | | |
| $h_1 = h_{EF}$ (hinge) to glass | 122 | 47 (6) | 32–78 | 43 | NS |
| $h_2 = h_{PS}$ (hinge) to glass | 20 | 86 (10) | 68–104 | 86 | NS |
| $h_3 = h_{PS}$ (hinge) to $h_{EF}$ (hinge) | 28 | 50 (11) | 26–56 | 43 | NS |
| Lattice membrane heights | | | | | |
| $h_4 = h_{EF}$ (smooth lattice) to glass | 56 | 108 (17) | 77–130 | 107 | NS |
| $h_5 = h_{EF}$ (smooth lattice) to $h_{EF}$ (hinge) | 76 | 69 (10) | 52–100 | 64 | NS |
| $h_6 = h_{PS}$ (lattice) to glass | 46 | 146 (14) | 104–173 | 150 | NS |
| $h_7 = h_{PS}$ (lattice) to $h_{EF}$ (smooth lattice) | 70 | 46 (7) | 18–52 | 43 | NS |
| $h_8 = h_{PS}$ (lattice) to $h_{PS}$ (hinge) | 11 | 58 (10) | 46–78 | 64 | NS |
| $h_9 = h_{PS}$ (lattice) to $h_{EF}$ (hinge) | 41 | 104 (18) | 78–130 | 107 | NS |

Numbers in parentheses after means are standard deviations.
*P*: The probability on the Student's *t* test (1, 43) that there is a significant difference between the sample observations and the predicted values.
NS: The predicted value is not significantly different at the 0.05 level from the sample of observations using a two tailed Student's *t* test.

TABLE III

*Parameters of Globular Lattice Membranes in Metallic Replicas on Glass*

| Designation | No. | Mean | Range | Expected value | *P* |
|---|---|---|---|---|---|
| | | | Å | | |
| $h_{4a} = h_{EF}$ (globular lattice maximum) to glass | 227 | 163 (24) | 96–234 | — | — |
| $h_{4b} = h_{EF}$ (globular lattice minimum) to glass | 90 | 120 (14) | 78–156 | 107 | NS |
| $h_{5a} = h_{EF}$ (globular lattice maximum) to hinge | 272 | 118 (17) | 78–182 | 120 (163 less 43) | NS |
| Corrected to glass (+43Å) | | 161 (17) | 123–227 | 163 | NS |
| $h_{5b} = h_{EF}$ (globular lattice minimum) to hinge | 42 | 76 (13) | 52–104 | 64 | NS |
| Corrected to glass (+ 43Å) | | 119 (13) | 95–147 | 107 | NS |
| $h_{5c}$ = height of globular lattice particle above smooth lattice | 154 | 55 (14) | 26–104 | 56 (163 less 107) | NS |

Numbers in parentheses after means are standard deviations.
*P* and NS: See Table II.

replication. We regard them as some kind of decorated plastic deformation artifact of the kind described long ago by Branton (5) and more recently by Sleytr and Robards (45).

## DISCUSSION

### General Interpretation

Our findings allow us to propose a three-dimensional model of the lattice membrane to a resolution of ~40 Å. It is comprised of lipids in a bilayer covered on its cytoplasmic side by a smooth layer of protein ~25–30 Å thick and on its external side by a hexagonal array of protein particles with a unit cell of 160 Å. Each protein particle is comprised of six identical subunits arranged around a central hole ~20 Å in diameter. The particle protrudes ~50–60 Å into the external medium making the overall membrane thickness ~140–150 Å. In FFE preparations the particle is reflected in the EF face by globular intramembrane particles (IMPs) ~120 Å in diameter. We consider this globular IMP to be an artifact of preparation for the following reasons: (*a*) It is thicker than the total membrane thickness. (*b*) There is no complementary structure in the PF face that can accommodate it. (*c*) There is no indication of substructure in the globular IMP. (*d*) In specimens prepared by a new technique the globular IMP is replaced by a new structure nearly complementary to the PF face. A paracrystalline structure is present in the lipid bilayer. The three-dimensional model deduced morphologically is compatible with chemical data gathered from isolated preparations (11, 27, 54).

### Alternate Interpretations

Other interpretations of our findings could be made. These rely on the presence of pits in the PF faces to accommodate the globular EF particles. It has indeed been stated repeatedly in previous reports (47, 30, 42) that pits were present in the PF faces. However, reexamination of the micrographs concerned shows the PF face patterns to be essentially the same as those analyzed here in more detail. The term pit as used in the earlier papers was not based on the kind of analysis we have done on these patterns. It was at first assumed by us (30) that depressions of sufficient depth were indeed present in the PF faces but were partially filled in by metal during shadowing. However, the detailed analysis presented here shows this to be incorrect. Also, Severs and Warren (42) commented on the fact that the PF pits were not large enough to accommodate the EF particles. However, they did not elaborate further on this. Staehelin et al. (47) also appreciated that the so-called pits were more complex.

Staehelin et al (47) considered the EF particles each to consist of a set of six cylinders, each roughly 50 Å in diameter surrounding a core of different material as estimated from their Fig. 22 (47). They showed the core material in their diagram as fracturing along with the center of the lipid bilayer and the particles each as a set of six elongated transmembrane cylinders that did not fracture, but rather were withdrawn from the cytoplasmic half of the lipid bilayer, leaving a set of six holes each ~50 Å in diameter around the central material. Some of our results could be explained in terms of this model. The globular particles we have observed could each be interpreted as groups of six cylindrical particles withdrawn from the PF face with plastic deformation and with decoration by metal obscuring the subunit structure and increasing their height to the degrees observed. The appearance of the PF face would be compatible with this interpretation if the holes made by the six subunits were partly filled in so that all that is seen is a shallow ring around the central residual material. Our smooth lattices then could be interpreted as regions in which the nonlipid subunits fractured cleanly in the middle of the bilayer. This has the attractive feature of offering a ready explanation for the relative resistance of the EF pattern to etching.

We consider the above interpretation to be unlikely for the following reasons. There are extensive areas of two distinctive types of pattern in the EF faces in our material, the globular and smooth lattices. If we regard the globular areas to be ones in which transmembrane particles were pulled out of the PF face and the smooth areas to be ones in which the transmembrane particles were simply fractured uniformly in the center of the bilayer, certain consequences are required in the PF faces in unetched preparations. There must be corresponding areas in the PF faces, one of which shows pits corresponding to the globular particles, and another resembling the smooth EF face. Instead we see only one pattern in the PF face, and it is like the one in Figs. 5–7. Another consequence of the above interpretation would be that the areas in the PF face from which the globular particles were not withdrawn but were cross fractured should be as resistant to etching as the EF face smooth lattice regions. This should result in two different kinds of pattern in the etched PF faces. Instead, again we see only one pattern. The PF face pattern is uniformly destroyed by etching. Hence this interpretation is not tenable.

Even if under other conditions true conical pits were to be demonstrated in a PF face, this would not affect our interpretation because such pits in sufficient numbers and regularity do not occur in our material. If they should appear in other material treated differently, different interpretations would be required for that material.

It might be argued that the metal that we have observed in

the center of each ring of metal in the PF faces is simply metal that has piled up in the center of deep pits. This proposition is eliminated by the patterns observed. If this were the case a single demilunar shadow would be cast into each pit perpendicular to and on the side of the direction of shadowing. This would vary in width with the degree of tilt, but would always have the same general features. This is not the kind of shadow obtained as can be seen in Figs. 5–7 *a* and *d*. Shadows are present on both sides of the central metal spot in the center of each repeating unit. This is visible in the unfiltered images (upper circle, Fig. 7 *a*), but it is more clear in the filtered image (Fig. 7 *d*). Here the spots of metal are each surrounded, albeit incompletely, by a dark shadow ring. If there is a structure in the center of each ring, there should be either a complete ring of shadow around it or a demilunar shadow cast on the side of the central material toward the metal source and a conical shadow from it perpendicular to the direction of shadowing, depending on the depth of the depression around the central material. This is essentially the case as can be seen in the filtered image (Fig. 7 *d*). The dark-shadow ring around each central metal spot is almost complete, although the shapes of the shadows are somewhat distorted. There is some interruption of the shadow ring by metal toward the lower right in Fig. 7 *d*. However, this is easily understood, bearing in mind that this surface was shadowed in a whole cell where the orientation was unknown, by supposing that the plane of the membrane is rotated to some degree around the line of shadowing. This could easily cause one side of the ring-shaped shadow to be partly filled in.

## Problems of Complementarity

In considering the complementarity of the EF and PF faces in the lattice membrane, we should make a clear distinction between the two kinds of patterns we see in the EF faces. Severs and Warren (42) measured the diameter of the globular IMP particle to be 121 ± 12 Å. We have measured the height of the particle and shown that it projects a mean distance of 55 Å above the plane of the smooth EF lattice. The globular IMP does not display substructure. In the smooth EF surface each globular particle is replaced by a domain with a more complex structure. Further, by contrast to the particle, the domain does not project above the fracture plane in the center of the bilayer. Instead, a portion of it is slightly depressed. The particles and the corresponding domains are therefore quite different. Fig. 16 is a diagram that should make this clear. In *a* the globular EF particles are drawn to the mean height in the globular lattice determined by our measurements ($h_{4a}$ in Table III). In *b* the domains are drawn in the lower membrane half to scale as they appear in the EF faces of the smooth lattice. The PF face of the upper membrane half is shown diagrammatically as it appears when shadowed at a low angle in unetched material. In the unfractured region these patterns are continued for clarity, but in fact they might well be smooth before fracture. The depressions could result from slight melting or differential collapse during replication. Consider the appearance of the PF face to be expected if it is to be complementary to each of the two kinds of EF faces. In Fig. 16 *b* the PF face is just as we see it in all the published micrographs in which a pattern is visible. The domains in the PF face correspond closely to the ones in the EF face in the smooth plaques. Each consists of an annular rim of metal around a central spot separated from the rim by a depression. The annular rims are wider (~40 Å) in the PF

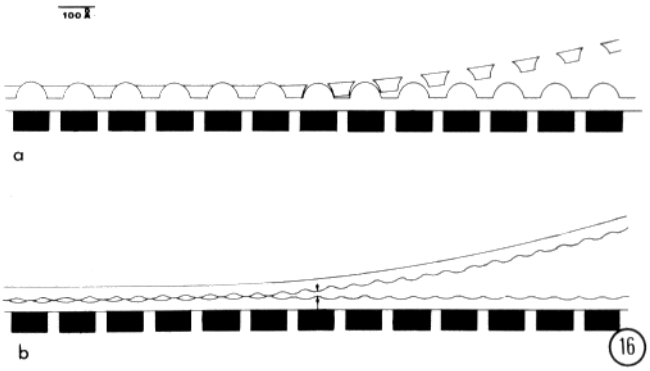


FIGURE 16 Cross-sectional diagrams of the lattice membrane with the external surface facing down. In *a* is shown the appearance to be expected if the globular pattern were real. The PF face above would have to contain deep pits that penetrate all the way through into the cytoplasm. This appearance of the PF face has not been seen by us. The lower diagram *b* shows the degree of complementarity of the EF and PF faces found in the smooth pattern regions. The lower arrow designates the raised center of an EF domain and the upper one that of the corresponding PF domain.

face, and are more complete and the central metal spot is larger (~60 Å) than the corresponding structures in the EF domains. The depressions in each surface are mirror images. Otherwise the surfaces correspond closely. In Fig. 16 *a*, in which the PF face is drawn to be complementary to the globular lattice, we see spherical pits ~120 Å in diameter penetrating the whole thickness of the protoplasmic half of the membrane. Such holes have not been observed in any published micrographs, no matter at what angle the shadowing material has been deposited. To be sure the shadowing angle influences the appearance of the PF plaques. Fig. 18 in reference 36 shows several plaques shadowed at different angles. The ones shadowed at high angles simply appear smooth and the lattice can only be detected by optical diffraction. At lower angles the lattices appear as in Figs. 5–7. Because the globular pattern is the dominant one, deep pits or holes should be the dominant pattern seen in the PF faces. When pits such as this actually exist in fracture faces, they are readily demonstrable as in gap junctions. Because they have not been demonstrated in the bladder membrane in any published micrographs, we conclude that they must not occur to any significant degree. This agrees with our conclusion that the commonly observed raised globular particles do not exist in the intact membranes. The globular particles seen in our preparations must be produced from the smooth lattice as an artifact at some point in the preparatory procedure. One might visualize them as being produced by some kind of plastic deformation of the EF lattice occurring during fracture or perhaps by some kind of explosion during fracture or subsequently during replication. Their height may be increased by decoration before and/or during replication and we have optical diffraction evidence for this. The important point is that the ~120 × 55 Å amorphous globular particle of the commonly observed EF face is an artifact in the sense that it does not exist as such in the native membrane, regardless of the exact nature of the artifact.

One further point about complementarity deserves comment. The PF and ES images in Figs. 7 *d* and 3 *d* are to some extent complementary. To a lesser degree, this also applies to the EF image in Fig. 4 *d*. It is curious that the regions in the ES that project and accumulate metal should correspond to depressed regions in both the fracture faces.

## Other Problems of Artifact

We have considered the obvious possibility that the smooth lattice is an artifact produced from the globular lattice by the procedures we have used. Perhaps the globular particles simply collapse into the smooth lattice either in $LN_2$ or during the prolonged etching, being altered just as the PF patterns are changed. We do not believe this to be the case for several reasons. First, the globular lattice should not be compared with the smooth PF lattice in this sense. The variations in contours in the globular lattice are at least an order of magnitude greater than those in the PF face lattice. Second, we have seen the smooth lattice in whole-cell preparations that have not been etched (Fig. 13). Third, Staehelin et al. (47) observed a limited area of this lattice at least once in their material. Finally, the smooth lattice is more nearly complementary to the PF lattice and the rough globular one is completely uncomplementary.

## Sensitivity of the PF Face

Considering the similarities in the patterns seen in the PF faces and the smooth EF faces it is curious that one, the PF face, should be very sensitive to etching and the other, the EF face, very resistant. The PF face pattern is rapidly destroyed during etching according to Staehelin et al (47) and Severs and Warren (42). Our results agree with these observations. The EF pattern in contrast withstands prolonged etching very well. This suggests that the constituents responsible for the observed patterns may differ significantly

## External Particle Lattice

The loose arrangement of particles between the compact plaques in Fig. 2 deserves some comment. This is an unusual appearance which might be an artifact induced by the isolation procedure or represent a stage in assembly of the lattice (42). We interpret it in any case as being an indication of fluidity in the membrane. Another manifestation of fluidity is the fact that the plaques in some of the isolated fractions are closer together, greatly reducing the total fractional area of hinge membrane (42). We have not made quantitative measurements, but there is obviously a significant reduction in the hinge membrane areas in membranes like the ones shown in Figs. 9 and 12 as compared with ones like Figs. 5, 8, 10, and 11. Whole plaques evidently can move in relation to one another, altering the relative area of hinge membrane as they do so. It would seem that this movement usually occurs without disruption of the regularity of the particles in the lattice, because the kind of picture seen in Fig. 2 is very rare.

## Nature of the Globular IMP

We cannot specify the exact nature of the globular IMPs but we believe them to be primarily plastic deformation artifacts of the kind described in a recent article by Sleytr and Robards (45). Their size evidently is exaggerated by decoration before and during replication (2). Decoration undoubtedly plays a significant role here but we believe the primary process to be plastic deformation. It may be that small plastic deformations of the lattice domains occur during fracture and that these decorate first with water during etching (8) and later with metal (2) during replication to exaggerate their size.

The globular IMPs seen in Figs. 6 and 7 on the PF faces support the latter interpretation. These particles occur mainly on the hinge membrane PF faces but also are seen on the lattice domains of the PF plaques, on adjacent smooth ice surfaces and on the intersection between ice and membrane surfaces. They are very variable in numbers and many hinge membrane PF faces are entirely free of them over the areas of many plaques. They thus lack specificity in size, location, and distribution. It seems most likely that this particular particle represents a water condensation artifact of the kind described recently by Gross and Moor (17) and Gross et al. (18). It is important that they appear in an unetched specimen.

The work reported here may be useful in the interpretation of the nature of IMPs in general. Franke has discussed the problem in making such interpretations with particular clarity (16). There is no doubt that polypeptide chains frequently traverse the lipid bilayer in membranes (31, 39–41, 58). There also seems little doubt that some protein molecules reside within the bilayer where they may form channels that mediate transport phenomena either within themselves or by aggregation as discussed by Singer (44) and shown to be the case in gap junctions (10, 32, 51, 59). The purple membrane of *Halobacterium halobium* is an extreme example of this (20, 48, 49, 50). Such transmembrane proteins may, of course, be related in some cases to the ubiquitous IMPs and indeed in some cases the IMP might literally be the protein molecule itself coated with metal. However, in the purple membrane individual bacteriorhodopsin molecules have not been resolved in FFE preparations. Only aggregates (3, 15, 52, and footnote 1) have been seen and these appear qualitatively different from the usual globular IMP like the ones seen in the bladder membrane. Recently, typical ~10-nm globular IMPs with pits in the complementary fracture faces have been produced experimentally in a pure lipid mixture of lecithin and cardiolipin in the presence of $Ca^{++}$ (56). Clearly it is important to decide whether or not one can identify a particular IMP in molecular terms on its morphological characteristics. The work reported here suggests that this should be done with great caution.

The authors wish to acknowledge many helpful discussions with Dr. William Longley and other colleagues. They also wish to thank Ms. Florence Stubbs and Ms. Susan Hester for technical assistance, and Ms. Wadeeah Beyah for photographic assistance. Special thanks are due to Dr. Ernst Helmreich of the Physiological Chemistry Institute of the University of Würzburg for the use of his departmental facilities and helpful discussions. Dr. T. H. Schiebler of the Anatomical Institute also provided electron microscopy facilities. Thanks are also due to Dr. W. Hoppe of the Max Planck Institut für Biochemie, Munich; Dr. Elmar Zeitler of the Fritz Haber Institut für Electronen Microscopie, Berlin; Dr. Fritz Miller of the Biochemistry Department of the University of Munich; and Sir John Kendrew of the European Molecular Biology Laboratory, Heidelberg who provided electron microscopy laboratory facilities for one of us, J. D. Robertson, during 1978–79.

The work was supported by National Institutes of Health Program Project grant 9 P01 GM NS 23911-06.

J. D. Robertson was on sabbatical leave in the Physiological Chemistry Institute, University of Würzburg, Würzburg, Federal Republic of Germany as a recipient of a Senior Scientist Award of the Alexander von Humboldt Society during the period in 1978–79 when this manuscript was written.

*Received for publication 26 November 1979, and in revised form 4 March 1980.*

## REFERENCES

1. Bailey, N. T. J. 1959. Statistical Methods in Biology. The English University Press Ltd., London.

[1] Robertson, J. D., W. Schreil, and M. Reedy. Unpublished results.

2. Basset, C. A., D. J. Blundell, and A. Keller. 1967. Surface structure of Polyethylene Crystals as revealed by surface decoration. I. Preliminary Survey. *J. Macromol. Sci. (Phys.)*. B1(1):161–184.
3. Blaurock, A. F., and W. Stoeckenius. 1971. Structure of the purple membrane. *Nat. New Biol.* 233:152–155.
4. Branton, D. 1966. Fracture faces of frozen membranes. *Proc. Natl. Acad. Sci. U. S. A.* 55: 1048–1056.
5. Branton, D. 1969. Membrane Structure. *Annu. Rev. Plant. Physiol.* 20:209–238.
6. Branton, D. 1971. Freeze-etching studies of membrane structure. *Phil. Trans. Roy. Soc.* B261:133–138.
7. Branton, D. 1973. The fracture process of freeze-etching. In Freeze-etching Techniques and Applications E. L. Benedetti and P. Favard, editors. Societe Francaise Microscopie Electronique, Paris. 107.
8. Branton, D., S. Bullivant, N. B. Gilula, M. J. Karnovsky, H. Moor, K. Mühlethaler, D. H. Northcote, L. Packer, B. Satir, P. Satir, V. Speth, L. A. Staehelin, R. L. Steere, and R. S. Weinstein. 1975. Freeze-etching nomenclature. *Science (Wash. D. C.)*. 190:54–56.
9. Bullivant, S. 1974. Freeze-etching techniques applied to biological membranes. *Phil. Trans. Roy. Soc. Lond.* B268:5–14.
10. Caspar, D. L. D., D. A. Goodenough, L. Makowski and W. C. Phillips. 1977. Gap junction structures. I. Correlated electron microscopy and x-ray diffraction. *J. Cell Biol.* 74:605–627.
11. Caruthers, J. S., and M. A. Bonneville. 1977. Isolation and characterization of the urothelial lumenal plasma membrane. *J. Cell Biol.* 73:382–399.
12. Chlapowski, F. J., M. A. Bonneville, and L. A. Staehelin. 1972. Lumenal plasma membrane of the urinary bladder. II. Isolation and structure of membrane components. *J. Cell Biol.* 53:92–104.
13. Costello, M. J., and J. M. Corless. 1978. The direct measurement of temperature changes within freeze-fracture specimens during rapid quenching in liquid coolants. *J. Microsc. (Oxf.)*. 112:17–37.
14. Fisher, K. A. 1975. "Half" membrane enrichment: verification by electron microscopy. *Science (Wash. D. C.)*. 190:983–985.
15. Fisher, K. A., and W. Stoeckenius. 1977. Freeze-fractured purple membrane particles: protein content. *Science (Wash. D. C.)*. 197:72–74.
16. Franke, W. W., E.-D. Jarasch, W. Herth, U. Scheer, and H. Zerban. 1974. A. Morphology. I. Cytology. a) General and Molecular Cytology. Progress in Botany/Fortschritte der Botanik 37. Springer-Verlag, New York.
17. Gross, H., and H Moor. 1978. Decoration of specific sites on freeze-fractured membranes. Ninth International Congress on Electron Microscopy, Toronto, Vol. II. 140–141.
18. Gross, H., O. Kuebler, E. Bas, and H. Moor. 1978. Decoration of specific sites on freeze-fractured membranes. *J. Cell Biol.* 79:646–656.
19. Gulik-Krzywicki, T., and M. J. Costello. 1978. The use of low temperature x-ray diffraction to evaluate freezing methods used in freeze-fracture electron microscopy. *J. Microsc. (Oxf.)*. 112:103–113.
20. Henderson, R., and P. N. T. Unwin. 1975. Three dimensional model of purple membrane obtained by electron microscopy. *Nature (Lond.)* 257:28–32.
21. Hereford, F. V., and D. H. Northcote. 1973. Fracture planes of the plasmalemma of some higher plants revealed by freeze-etch. *J. Cell Sci.* 23:621–635.
22. Hicks, R. M. 1965. The fine structure of the transitional epithelium of rat ureter. *J. Cell Biol.* 26:25–48.
23. Hicks, R. M. 1966. The junction of the Golgi complex in transitional epithelium. Synthesis of the thick cell membrane. *J. Cell Biol.* 30:623–643.
24. Hicks, R. M. 1966. The permeability of rat transtional epithelium. Keratinization and the barrier to water. *J. Cell Biol.* 28:21–31.
25. Hicks, R. M., and B. Ketterer. 1969. Hexagonal lattice of subunits in the thick luminal membrane of the rat urinary bladder. *Nature (Lond.)*. 224:1304–1305.
26. Hicks, R. M., and B. Ketterer. 1970. Isolation of the plasma membrane of the luminal surface of rat bladder epithelium and the occurrence of a hexagonal lattice of subunits both in negatively stained whole mounts and in sectioned membranes. *J. Cell Biol.* 45: 542–553.
27. Hicks, R. M., B. Ketterer, and R. C. Warren. 1974. The ultrastructure and chemistry of the luminal plasma membrane of the mammalian urinary bladder: a structure with low permeability to water and ions. *Phil. Trans. R. Soc. Lond. B.* 268:23–38.
28. Ibanez, N., A. Candiotti, R. O. Calderon, and B. Moni. 1974. Carbohydrate components of plasma membrane of transitional epithelium of urinary tract. *Experientia (Basel)*. 30: 477–480.
29. Ketterer, B., R. M. Hicks, L. Christodoulides, and D. Beale. 1973. Studies of the chemistry of the luminal plasma membrane of rat bladder epithelial cells. *Biochim. Biophys. Acta.* 311:180–190.
30. Knutton, S., and J. D. Robertson. 1976. Regular structures in membranes: the lumenal plasma membrane of the cow urinary bladder. *J. Cell Sci.* 22:355–370.
31. Kyte, J. 1975. Structural studies of sodium and potassium activated adenosine triphosphatase. *J. Biol. Chem.* 250:7443–7449.
32. Makowski, L., D. L. D. Caspar, W. C. Phillips, and D. A. Goodenough. 1977. Gap junction structures. II. Analysis of the x-ray diffraction data. *J. Cell Biol.* 74:629–648.
33. Minsky, B. D., and F. J. Chlapowski. 1978. Morphometric analysis of the translocation of lumenal membrane between cytoplasm and cell surface of transitional epithelial cells during the expansion-contraction cycles of mammalian urinary bladder. *J. Cell. Biol.* 77: 685–697.
34. Nanninga, N. 1969. Observation of the ultrastructure of *Bacillus subtilis* by chemical fixation as verified by freeze-etching. *J. Cell Biol.* 42:733–744.
35. Nanninga, N. 1971. Uniqueness and location of the fracture plane in the plasma membrane of *Bacillus subtilis*. *J. Cell Biol.* 49:564–570.
36. Porter, K. R., and M. A. Bonneville. 1963. An introduction to the fine structure of cells and tissues. Lea and Febiger, Philadelphia.
37. Porter, K. R., K. Kenyon, and S. Badenhausen. 1967. Specialization of the unit membrane. *Protoplasma*. 63:262–274.
38. Robertson, J. D. 1972. The structure of biological membranes. *Arch. Int. Med.* 129:202–228.
39. Rothman, J. E., and E. P. Kennedy. 1977. Asymmetrical Distribution of Phospholipids in the Membrane of *Bacillus megaterium*. *J. Mol. Biol.* 110:603–618.
40. Rothman, J. E., and J. Leonard. 1977. Membrane assymetry. *Science. (Wash. D. C.)*. 195: 743–753.
41. Ruoho, A., and J. Kyte. 1974. Photoaffinity labeling of the ouabain-binding side in ($Na^+ + K^+$) adenosinetriphosphatase. *Proc. Natl. Acad. Sci. U. S. A. PNAS (USA)* 71:2352–2356.
42. Severs, N. J., and R. C. Warren. 1978. Analysis of membrane structure in the transitional epithelium of rat urinary bladder. 1. The luminal membrane. *J. Ultrastruct. Res.* 64:124–140.
43. Simpson, G. G., Anne Roe, and R. C. Lewontin. Revised 1960. Quantitative Zoology. Harcourt Brace, Inc., New York.
44. Singer, S. J. 1974. The molecular organization of membranes. *Annu. Rev. Biochem.* 43: 805–833.
45. Sleytr, U. B., and A. W. Robards. 1977. Plastic deformation during freeze-cleavage: a review. *J. Microsc. (Oxf.)*. 110:1–26.
46. Sommer, J. R. 1977. To Cationize glass. *J. Cell Biol.* 75(2, Pt. 2):245*a* (Abstr.).
47. Staehelin, L. A., F. J. Chlapowski, and M. A. Bonneville. 1972. Lumenal plasma membrane of the urinary bladder. I. Three-dimensional reconstruction from freeze-etch images. *J. Cell Biol.* 53:73–91.
48. Stoeckenius, W., and R. Rowen. 1967. A morphological study of *Halobacterium halobium* and its lysis in media of low salt concentration. *J. Cell Biol.* 34:365–393.
49. Stoeckenius, W., and W. H. Kunau. 1968. Further characterization of particulate fractions from lysed cell envelopes of *Halobacterium halobium* and isolation of gas vacuole membranes. *J. Cell Biol.* 38:337–357.
50. Unwin, P. N. T., and R. Henderson. 1975. Molecular Structure Determination by Electron Microscopy of Unstained Crystalline Specimens. *J. Mol. Biol.* 94:425–440.
51. Unwin, P. N. T., and G. Zampighi. 1980. Structure of the junction between communicating cells. *Nature (Lond.)*. 283:543–549.
52. Usukura, J., E. Yamada, F. Tokunaga, T. Iwasa, and T. Yoshizawa. 1978. Ultrastructure of purple membrane of *Halobacterium halobium*. Proceedings of the Sixth International Biophysics Congress, Kyoto, Japan.
53. Vergara, J. 1969. A freeze-etch study of the unit membranes of mouse urinary epithelial cells. *Anat. Rec.* 163:280.
54. Vergara, J., W. Longley, and J. D. Robertson. 1969. A hexagonal arrangement of subunits in membrane of mouse urinary bladder. *J. Mol. Biol.* 46:593–596.
55. Vergara, J., F. Zambrano, J. D. Robertson, and H. Elrod. 1974. Isolation and characterization of luminal membranes from urinary bladder. *J. Cell Biol.* 61:83–94.
56. Verkleij, A. J., C. Mombers, J. Leunissen-Bijvelt, and P. H. J. Th. Ververgaert. 1979. Lipidic intramembranous particles. *Nature (Lond.)*. 279:162–163.
57. Warren, R. C., and R. M. Hicks. 1970. Structure of the subunits in the luminal membrane of the rat urinary bladder. *Nature (Lond.)*. 227:280–281.
58. Whiteley, H. M., and H. C. Berg. 1974. Amidination of the outer and inner surfaces of the human erythrocyte membrane. *J. Mol. Biol.* 87:541–561.
59. Zampighi, G., and P. N. T. Unwin. 1979. Two forms of isolated gap junctions. *J. Mol. Biol.* 135:451–464.